Journal of Materials Chemistry C

Accepted Manuscript

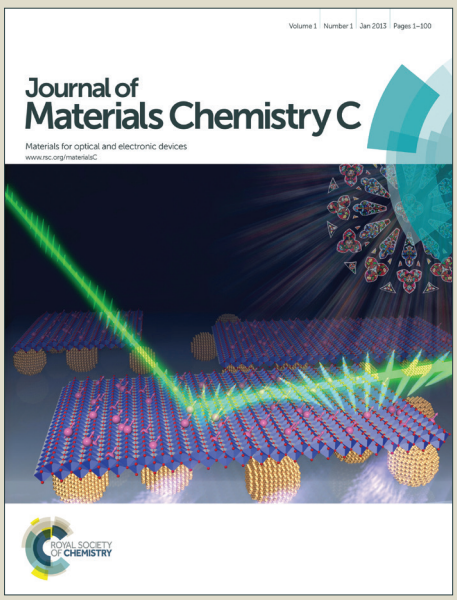

ROYAL SOCIETY OF CHEMISTRY

www.rsc.org/materialsC

Journal of Materials Chemistry C

RSCPublishing

ARTICLE

Preparation and enhanced electro-responsive characteristic of graphene/layered double-hydroxide composite dielectric nanoplates

Cite this: DOI: 10.1039/x0xx00000x

Received 00th January 2012,
Accepted 00th January 2012

DOI: 10.1039/x0xx00000x

www.rsc.org/

Yuezhen Dong[a], Yang Liu[a], Jianbo Yin[a,*] and Xiaopeng Zhao[a,*]

To combine the advantages of conducting graphene nanosheet (GNS) and insulating layered inorganic, we use a simple one-pot hydrothermal method to prepare two-dimensional dielectric nanoplates composed of GNS/Mg-Al layered double-hydroxide (GNS/LDH) composite for use as novel anisotropic electro-responsive electrorheological (ER) material. The structure of samples is characterized by Fourier transform infrared spectra, X-ray diffraction pattern, X-ray photoelectron spectroscopy, Raman spectrum, and scanning electron microscopy. The conductivity and dielectric property are measured by impedance analyzer and the electro-responsive ER characteristic of GNS/LDH composite dispersed in insulating oil is characterized by rheometer. The results demonstrate that the LDH can provide electrically insulting effect for GNS, while the incorporation of conducting GNS can enhance the dielectric polarization of LDH. The GNS/LDH composite shows significantly stronger ER effect compared to the pure LDH especially under AC electric fields due to the enhanced polarization response.

Introduction

Since the pioneering discovery by Gaim et al.,[1] graphene has attracted a lot of scientific interests because of its atomically thick two-dimensional (2D) structure, excellently physical properties, and easy mass production. Not only has the individual graphene nanosheet (GNS) been used to fabricate nanodevices such as field-effect transistors, nanosensors, and plasmonics, but also the incorporation of GNS into various matrices has produced advanced composite materials with improved electrical, mechanical, and thermal properties.[2] On the other hand, due to some unique characteristics of GNS, such as small size, large aspect ratio, thermal, electronic, and transport properties, GNS-based colloid dispersions have been studied for various applications such as thermal transfer fluids, liquid crystal, and so on.[3,4]

Recently, a growing attention has focused on GNS and its oxide as the active components or fillers of electro-responsive electrorheological (ER) suspensions owing to its high-aspect-ratio structure and excellently electrical property.[5-11] ER suspensions, consisting of polarizable particles in electrically insulating oil, are a type of important smart fluids with electrically tunable rheological characteristic. They have potential uses as electrical–mechanical interfaces for the active-control of various devices because of technical advantages, such as rapid response time, reversibility, and low power consumption.[12] However, the conventional ER suspensions are mainly based on micro-size particles and they often subject to large particle sedimentation problem. Recent researches of using nanoparticles as the dispersal phase has led considerable interests in developing non-conventional ER suspensions.[12] In particular, significant attentions have been paid to ER suspensions based on elongated anisotropic nanoparticles, such as nanotubes, nanofibers and nanoplates.[8-10,13-20] It is found that the anisotropic nanoparticles have exhibited not only enhanced ER characteristic, but also reduced particle sedimentation compared to the conventional suspensions of spherical particles. At the same time, the analogues ER enhancement has also been observed in elongated micro-size particles recently.[21,22] The property enhancements originate from the nature of elongated particles, e.g., large aspect ratio and anisotropic electronic properties. As one of the most popular 2D anisotropic nanomaterials, GNS shows potential as novel components or fillers of ER suspensions.[5-11] Unfortunately, pure GNS in itself is not suitable for ER suspension application because its high conductivity is easy to cause large current leaching and power consumption. Coating GNS with semi-conducting polymer (e.g. polyaniline, polypyrrole) or insulting inorganic (e.g. SiO_2, TiO_2) has been found to be able to effectively restrain the high conductivity of GNS.[8-11] However, the preparation techniques involving nano-coating are often complex and low yield, which largely limit the further application of the GNS-based ER materials. On the other hand, besides GNS, other layered materials (e.g., clay, hydroxide, and double-hydroxide) have also received wide investigation as the fillers of plastics and ER

suspensions because of their low cost and anisotropic morphology.[23-29] For example, the percolation network of layered double-hydroxide (LDH) plates in polystyrene has enhanced the rheological and dielectric behavior of composite.[24] However, for ER suspensions the ER effect of the layered inorganic materials is too weak to satisfy the requirement of application.[27-29]

In this paper, to attempt to combine the advantages of GNS and layered inorganic, we use a simple one-pot hydrothermal method to prepare novel dielectric nanoplates composed of chemically converted graphene nanosheet/Mg-Al layered double-hydroxide (GNS/LDH) composite for use as anisotropic 2D ER material. The method is simple and high yield. The composite material shows unique characteristics including high-aspect-ratio 2D plate-like morphology, low conductivity and enhanced dielectric polarization because the non-conducting LDH can provide electrically insulting effect for GNS, while the incorporation of conducting GNS can enhance the polarization response of LDH. Under electric fields, the GNS/LDH composite nanoplates when dispersed in insulating silicone oil show a strong electro-responsive characteristic. The field-induced ER effect of GNS/LDH suspension is significantly stronger than that of pure LDH suspension due to the enhanced dielectric polarization. The influences of electric field strength, frequency, and GNS content on ER characteristic have also been investigated.

Experimental section

Materials

$Mg(NO_3)_2 \cdot 6H_2O$, $Al(NO_3)_3 \cdot 9H_2O$, hexamethylenetetramine, and natural graphite plates with mean size of ~20 μm were purchased from Sinopharm Chemical Reagent Co. Ltd. of China. All the chemicals were of analytical grade and were used without further purification.

Fabrication of GNS/LDH composite nanoplates

Firstly, graphene oxide (GO) was synthesized from natural graphite plates according to an improved Hummers method [30] and then was diluted to form 5 mg/mL of GO colloid dispersion (pH=5-6) by ultrasonic treating for 30 min at frequency of 40 kHz and power of 100 W. *Then*, 25 g GO colloid dispersion was mixed with 80 mL of aqueous solution containing 5.120 g of $Mg(NO_3)_2 \cdot 6H_2O$ (0.020 mol), 3.750 g of $Al(NO_3)_3 \cdot 9H_2O$ (0.010 mol), and 3.640 g of hexamethylenetetramine (0.026 mol) under ultrasonic. After ultrasonic for 1 h, the mixture was transferred into a Teflon-lined stainless autoclave and was further heated at 140℃ for 12 h.[31] *Finally*, the black precipitate was separated, washed, and dried in vacuum to obtain resulting GNS/LDH composite (Here, the yield of the typical 10 wt% GNS/LDH composite was ~2.0 g. No Mg^{2+}/Al^{3+} ions were residual by titration with NaOH solution. The ratio of Mg/Al was ~1.94 according to Inductively Coupled Plasma result (ICP, IRIS), which was close to that of Mg/Al used in the experiments. These indicate that the preparation method is high yield.). The mass ratio of GNS/LDH in the composite could be controlled by the amount of initial GO. For comparison, pure Mg-Al LDH plates were also prepared by the same process except for GNS.

Preparation of ER suspensions

The GNS/LDH composite and pure LDH nanoplates were further dried for 48 h at 150℃ in vacuum and then quickly dispersed into dry silicone oil (Dielectric constant of ~2.7, viscosity of 50 mPa·s, density of 0.96 g/cm^3 at 25 ℃) to form ER suspensions. The volume fraction of nanoplates in suspensions was defined by the ratio of the volume of nanoplates to the total volume of suspensions. The nanoplate density was measured by a pycnometer filled with water at room temperature. To decrease the effect of porosity on density measurement, the pycnometer was placed in an ultrasonic cleaning bath and connected to a vacuum pump. After ultrasonic for 10 min under reduced pressure, the density was measured. The density is ~1.78 g/cm^3 for LDH and ~1.99 g/cm^3 for 10 wt% GNS/LDH composite.

Characterization and measurements

The chemical groups of samples were determined by the Fourier transform infrared spectra (FT-IR, JASCO FT/IR-470 Plus) in the range 400-4000 cm^{-1} at 4 cm^{-1} resolution. The structure was determined by the powder X-ray diffraction pattern (XRD, Philips X'Pert Pro) with a CuK_α irradiation at 40 kV/35 mA. The surface and chemical state were analyzed by X-ray photoelectron spectroscopy (XPS, Thermo Scientific K-Alpha) with a monochromatic AlK_α source. The C1s peak at 284.6 eV of the surface adventitious carbon was referred for all the binding energies in XPS. Raman measurements were carried out using Micro-Raman spectrometer (Raman, invia) at 532 nm. The morphology was observed by the scanning electron microscopy (SEM, JSM-6700F) at an accelerated voltage of 20 kV. The weight fraction of GNS in the GNS/LDH composite was determined by dissolving the GNS/LDH composite in HCl solution to remove the LDH.

The conductivity of GNS was high and it was directly measured by a four-point method (RTS-8). Since the conductivity of both LDH and GNS/LDH composite were low and they were layered and high-surface-area, in order to avoid the influences of moisture and porosity on the conductivity and dielectric properties when using powder method, we measured the conductivity and dielectric properties of their suspensions. In the conductivity measurement, a galvanometer was used to measure the current density of suspensions and then the conductivity of suspensions was determined according to $\sigma = j/E$, where j is the current density through suspensions and E is the electric field strength. Here, 1.0 kV/mm of electric field was applied to suspensions and, thus, the dispersed particles could form fibrous-like structure and this solidified suspension was analogous to fibrous microcomposite. Thereby, the conductivity of particles could be calculated by the following approximate mixture conductivity equation (1):[32,33]

$$\sigma = \phi \sigma_p + (1 - \phi)\sigma_f \quad (1)$$

where, σ is the conductivity of suspensions, σ_p is the conductivity of dispersed LDH or GNS/LDH, σ_f is the conductivity of used silicone oil, and ϕ is the volume fraction of particles in suspensions.

In the dielectric measurement, an impedance analyzer (HP 4284A) with a liquid measuring fixture (HP 16452A) was used to measure the dielectric constant and loss tangent in the frequency range of 20-10^6 Hz. Here, 1 V of bias electrical potential was applied during measurement. Thus, no fibrous-like structure formation or no interparticle interaction within suspensions was induced and, as a result, we could well understand the interfacial polarization of particles in medium oil. The dielectric parameters were determined by the fit of the Cole-Cole equation as shown in the following equation (2):[34]

$$\varepsilon^* = \varepsilon' + i\varepsilon'' = \varepsilon'_\infty + \frac{\varepsilon'_0 - \varepsilon'_\infty}{1 + (i\omega\lambda)^{1-\alpha}} \quad (2)$$

where, ε^* is the complex permittivity of suspension, ε'_0 and ε'_∞ are the limit values of the relative permittivity at the frequencies below and above the relaxation frequencies, respectively, ω is an angle frequency, λ is a dielectric relaxation time reflecting the rate of interfacial polarization, and α is the scattering degree of relaxation time.

Under electric fields, the fibrous-like ER structure of dispersed particles formed between two electrodes was observed by an optical microscopy (Nikon ALPHAPHOT-2). The ER characteristic of suspensions were measured by a stress-controlled rheometer (Thermal-Haake RS600) with a parallel plate system with diameter of 35 mm and gap of 1.0 mm, DC and AC high-voltage generators, oil bath system, and PC computer. Steady shear flow curves of shear stress-shear rate were measured by the controlled shear rate (CSR) mode within 0.1 - 1000 s^{-1} at room temperature. Before each measurement, we presheared the fluids for 60 s at 300 s^{-1} and then applied electric fields for 30 s to ensure the formation of equilibrium gap-spanning ER structures of dispersed particles before shearing. The static yield stress, which was defined as the maximum shear stress that made a solidified ER fluid start to flow,[35] was approximately obtained with the maximum shear stress in the low shear rate region according to flow curves.

Results and discussion

Fig. 1 shows the FTIR spectra of samples. The GO shows characteristic absorption bands at 3408, 1735, 1630, 1403, 1228, and 1054 cm^{-1}, which are assigned to the O-H, carbonyl C=O, aromatic C=C, epoxy C-O and alkoxy C-O stretching vibrations, respectively.[30] After the GO is hydrothermally treated, the bands of the oxygen functional groups almost disappear and the FTIR spectra only displays three weak bands at 3435, 1568 and 1183 cm^{-1} corresponding to the O-H, aromatic C=C and C-O stretching vibrations, respectively (see Fig. 1(b)). This indicates that the GO can be reduced into GNS during hydrothermal treatment.[36] The pure Mg-Al LDH shows that the characteristic bands at 3445, 1620 cm^{-1} due to the stretching and bending vibrations of the -OH between LDH layers, at 1351 cm^{-1} due to the vibration of CO_3^{2-} between LDH layers, and at 400-800 cm^{-1} due to Mg-O and Al-O vibrations.[31] For the typical GNS/LDH composite with CNS content =10 wt%, almost all the characteristic bands corresponding to LDH are observed but no significant absorption bands from GNS appears (see Fig. 1(d)). This may be due to the low content and weak IR absorption characteristic of GNS.

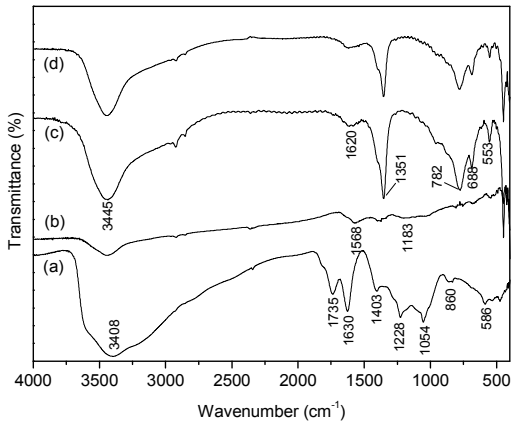

Fig. 1 FTIR spectra of samples: (a) GO; (b) GNS; (c) LDH; (d) 10 wt% GNS/LDH composite.

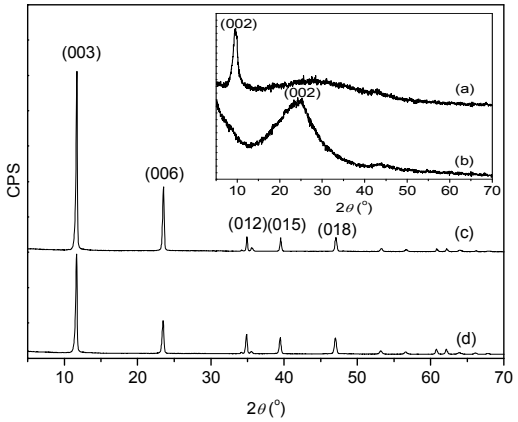

Fig. 2 XRD patterns of samples: (a) GO; (b) GNS; (c) LDH; (d) 10 wt% GNS/LDH composite.

Fig. 2 shows the XRD patterns of samples. The GO shows a broad and strong diffraction peak at 2θ =~9.50°, corresponding to the typical (002) plane of GO.[30] After the GO is hydrothermally treated, the XRD pattern (Fig. 2 (b)) gives an abroad strong diffraction peak at ~24.0° and a weak diffraction peak at ~43.5°, corresponding to the typical (002) and (100) planes of graphite. This indicates that the hydrothermal treatment can remove the oxygen-containing functional groups on the surface of GO and the GO has converted into GNS.[37] This is also in accordance with the FTIR result. The pure LDH shows sharp and symmetric XRD peaks at 11.6, 23.4, 34.8, 39.0, 47.1, and 61.4°, corresponding to the basal spacing of

(003), (006), (012), (015), and (018) of the layered Mg–Al LDH plates.[31] The XRD pattern of typical 10 wt% GNS/LDH composite is mainly composed of LDH phase. Compared with the pure LDH, however, there is a significant decrease in the peak intensity of GNS/LDH composite. It indicates that the incorporation of GNS has compressed the crystalline size, which can also be confirmed by the SEM observation in Figs. 3 and 4. Note that no characteristic peak of GNS at 2θ =~24.0° is observed in GNS/LDH composite, which can be attributed to the low content and the thin-layer characteristic of GNS in the GNS/LDH composite.

Fig. 3 shows the morphology of LDH and 10 wt% GNS/LDH composite. It is found that the pure LDH is of hexagonal plate with the lateral size of 5-10 μm and the thickness of 100-150 nm. From the high-resolution image in Fig. 3(c), one can see that the surface of pure LDH is clean and smooth. The GNS/LDH composite also shows hexagonal plate-like morphology. However, the lateral size is decreased to 3-5 μm and the thickness is decreased to 50-100 nm. This indicates that the incorporation of GNS has restrained the growth of LDH, which may be due to the fact that the presence of small-size GO has provided more nucleation centers for LDH formation compared to homogeneous nucleation process. As the GNS content increases, the lateral size and thickness of GNS/LDH composite further decrease (see Fig. 4), also supporting this point. Furthermore, from the high-resolution SEM image in Fig. 3(e) and (f), we can see that the wrinkled GNS is firmly attached on the surface of LDH, indicating the formation of GNS/LDH composite. This can be attributed to the fact that the negatively charged surface of GO provides Mg^{2+}/Al^{3+} cations with strong electrostatic absorption force, and leads to an in-situ growth of positively charged LDH on the surface of GO as shown in the schematic illustration of Fig. 5.[38] Meanwhile, the GO is reduced into GNS simultaneously. In addition, from Fig. 3 it can be found that no free GNS is observed when the content of GNS is relatively low. When the content of GNS increases is too high (>~20 wt%) (not shown here), however, the free naked GNS appears. This is harmful for ER suspension application because in this condition the small size LDH is unable to provide insulating effect for the GNS and the free GNS easily results in dielectric breakdown under electric fields. Therefore, the appropriate GNS content is needed.

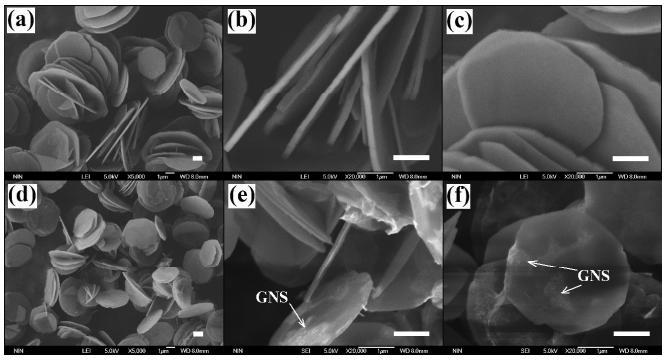

Fig. 3 SEM images of samples: (a-c) pure LDH; (d-f) 10wt% GNS/LDH composite (Scale bar=1 μm).

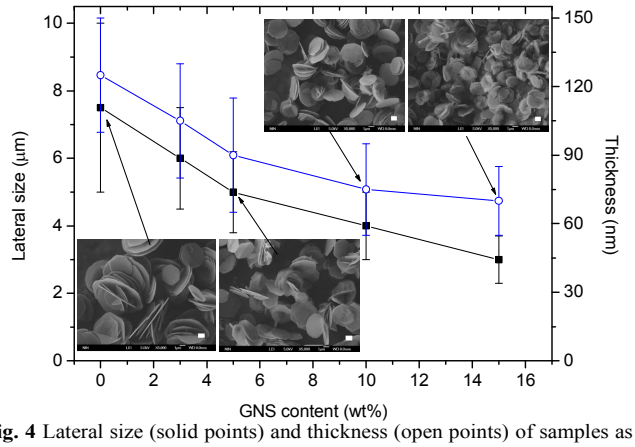

Fig. 4 Lateral size (solid points) and thickness (open points) of samples as a function of GNS content (Scale bar=1 μm in inserted SEM images).

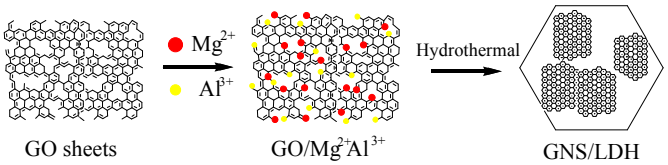

Fig. 5 Schematic illustration of the formation of GNS/LDH composite.

To clarify the chemical state of GNS in the GNS/LDH composite, XPS and Raman spectra were measured. As shown in Fig. 6(A), the deconvolution of the core-level C1s XPS spectrum of GO shows types of carbon bonds including C=C/C-C (284.6 eV), C–O (286.9 eV), and O–C=O (289.0 eV). After the GO is hydrothermally treated, the intensity of C=C/C–C bond (284.6 eV) increases and the intensity of bonds corresponding to oxidized carbon (C–O at 286.9 eV and O–C=O at 289.0 eV) obviously decreases, indicating that the GO has been deoxygenated to form GNS.[36] The deconvolution of the core-level C1s spectrum of GNS/LDH composite also shows strong C=C/C–C bond (284.6 eV) and weak oxidized carbon bonds (C–O and O–C=O), which infers that the GO has been reduced simultaneously during the in-situ growth of LDH on the surface and, thus, the hybrid GNS/LDH composite is formed. Raman spectroscopy is also an effective tool to determine the structural variations of carbonaceous materials. As shown in Fig. 6(B), three samples all show the D band at ~1350 cm^{-1} arising from the breathing mode of sp^2 carbon atoms in rings and the G band at ~ 1600 cm^{-1} arising from the bond stretching of all pairs of sp^2 carbon atoms in both rings and chains.[39] The Raman spectra of GNS/LDH composite also shows weak feature peaks of LDH at ~560 and ~1080 cm^{-1}, indicating the coexistence of GNS and LDH. Furthermore, the intensity ratio (I_D/I_G) of D band to G band reflects disorder degree and average size of the sp2 carbon domains.[39] The I_D/I_G values of GNS and 10 wt% GNS/LDH composite are 1.01 and 1.03 respectively, which are higher than 0.87 of GO. The similar result has also been observed in other GNS/LDH composites.[40,41] This has been considered to be attributed to the decrease of the size of the in-plane sp^2 domains due to the reduction of GO and the reestablishment of graphene network after removing the oxygen functional groups.[40,41] Therefore, the

GO does has been reduced into GNS simultaneously during the in-situ growth of LDH on its surface. It is also in accordance with the XPS result.

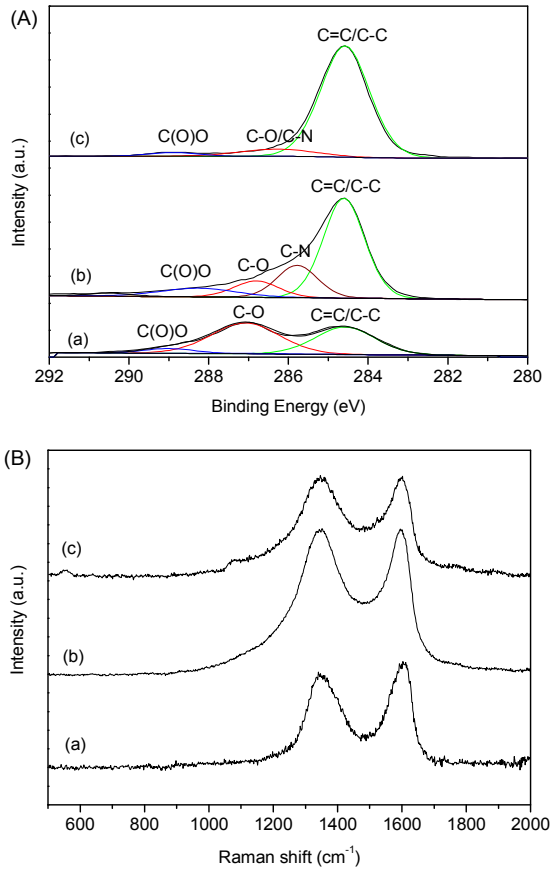

Fig. 6 (A) Deconvolution of core-level C1s XPS spectrum and **(B)** Raman spectrum of samples: (a) GO; (b) GNS; (c) 10 wt% GNS/LDH composite.

The DC conductivity of pure GNS is ~0.52 S/cm, which is too high to use as dispersal phase of ER suspensions due to easy dielectric breakdown under electric fields. However, the conductivity of GNS/LDH composite is largely decreased (see Table 1). For example, the conductivity of typical 10 wt% GNS/LDH composite is ~1.3×10^{-10} S/cm, which is very suitable for ER suspension applications according to the proposed ER mechanisms.[42] This indicates that the LDH has provided electrically insulting effect for the GNS due to the separable effect and, thus, the GNS cannot directly contact each other under electric field. As the GNS content increases, the conductivity of GNS/LDH composite increases. On the other hand, the incorporation of GNS can influence the dielectric property of LDH. As shown in Table 1, the dielectric constant increment ($\Delta\varepsilon'=\varepsilon'_0-\varepsilon'_\infty$) of the typical 10 wt% GNS/LDH suspension is ~2.56, which is about twice as high as that ($\Delta\varepsilon'$=1.43) of the pure LDH suspension. The dielectric relaxation time ($\lambda=1/(2\pi f_{max})$) of the 10 wt% GNS/LDH suspension is ~5.3×10^{-6} s, which is much faster than that (λ=~1.6×10^{-4} s) of the pure LDH suspension. It indicates that the GNS/LDH composite has larger polarizability and faster polarization response compared to the pure LDH. This dielectric enhancement can be attributed to the incorporation of the conducting GNS into LDH because it has been reported that introducing a conducting component can largely enhance the polarizability and polarization rate of composites.[43] When the GNS content is too high (> ~20 wt%), the free GNS appears and the conductivity of GNS/LDH composite rapidly elevates and the dielectric property cannot be measured due to large leaking conduction. It is not suitable to use as dispersal phase of ER suspensions due to large percolating current. Therefore, by a one-pot hydrothermal method, the GNS/LDH composite dielectric nanoplates have been prepared, in which the LDH layers can provide effectively insulting effect for GNS, while the incorporation of conducting GNS with an appropriate content of GNS can enhance the polarization response of LDH. The characteristics including high-aspect-ratio, enhanced polarization, and simple preparation allow the GNS/LDH composite nanoplates to have potential use as high-performance ER material. In the following, we investigate the electro-responsive ER property of GNS/LDH composite nanoplates when dispersed in insulating silicone oil.

Table 1. Conductivity and dielectric property of LDH and GNS/LDH suspensions (ϕ =~7.5 vol%, T=23°C).

Material	ε'_0	ε'_∞	$\Delta\varepsilon'$[a]	ε''[b]	λ(s)[c]	σ_p(S/cm)[d]
LDH	4.51	3.08	1.43	0.26	1.6×10^{-4}	$<10^{-12}$
3wt% GNS/LDH	5.01	3.17	1.84	0.27	1.3×10^{-5}	~3.4×10^{-11}
5wt% GNS/LDH	5.38	3.19	2.19	0.30	8.1×10^{-6}	~5.7×10^{-11}
10wt% GNS/LDH	5.79	3.23	2.56	0.39	5.3×10^{-6}	~1.3×10^{-10}
15wt% GNS/LDH	5.85	3.30	2.55	0.33	1.2×10^{-7}	~ 8.0×10^{-9}

[a] The dielectric constant increment of suspensions calculated by $\Delta\varepsilon'=\varepsilon'_0-\varepsilon'_\infty$; [b] The dielectric loss factor of suspensions at the frequency (f_{max}) of dielectric relaxation peak; [c] The dielectric relaxation time of suspensions calculated by $\lambda=1/(2\pi f_{max})$; [d] The DC conductivity of particles calculated by equation (1).

Fig. 7 shows the optical microscope of the suspension of typical 10 wt% GNS/LDH composite nanoplates in silicone oil without and with an external electric field. It is seen that, when the electric field is applied, the randomly dispersed GNS/LDH can rapidly contact each other to form gap-spanning fibrous structure between electrodes, indicating that the GNS/LDH has a good electro-responsive ER characteristic. This gap-spanning fibrous-like structure, which is dominated by sufficient electrostatic interaction between GNS/LDH composite nanoplates, will provide a large resistance to the shear flow perpendicular to electric field and thus enhance shear stress or viscosity of suspension.

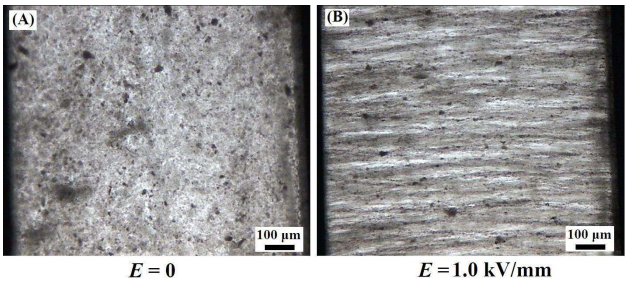

Fig. 7 Optical photo of the suspension of 10 wt% GNS/LDH composite in silicone oil without and with an AC electric field with frequency of 1 kHz (ϕ =~7.5 vol%, T=23°C)

Fig. 8 shows the real-time response of shear stress of the 10 wt% GNS/LDH suspension when an AC electric field with frequency of 1 kHz alternately turns on and off. When the electric field is applied, the shear stress of the suspensions increases rapidly. The value of shear stress is close to ~980 Pa at 2.0 kV/mm, which is 14 times that of the off-field shear stress of ~68 Pa. When the electric fields are removed, the shear stress rapidly declines back to the original level. As the electric field strength is increased, the shear stress increases and the real-time response of shear stress is still reversible, revealing good electro-responsive characteristic of the GNS/LDH composite. In particular, it is noted that the value of field-induced shear stress of the GNS/LDH suspension is 2.5 times as high as that of the pure LDH suspension, revealing that the GNS/LDH composite has stronger ER effect compared to the pure LDH.

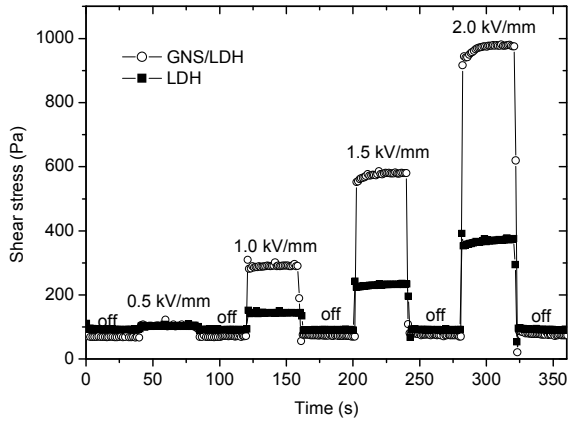

Fig. 8 Effect of switching an AC electric field with frequency of 1 kHz on the real-time response of the shear stress for 10 wt% GNS/LDH suspension and pure LDH suspension at shear rate of 100 s^{-1} (ϕ =15 vol%, T=23°C).

Fig. 9 shows the flow curves of shear stress vs. shear rate for the 10 wt% GNS/LDH suspension and pure LDH suspension at the same particle volume fraction. In the absence of an electric field, the flow curves of both suspensions departure from the Newtonian fluid behavior and show shearing thin. The off-field viscosity of the GNS/LDH suspension is higher than that of the pure LDH suspension at low shear rate region but lower than that of the later at high shear rate region. This reveals that the shear-thin behavior of the GNS/LDH suspension is more significant than that of the pure LDH suspension, which may be originated from the smaller particle size of GNS/LDH composite.[44] In the presence of an electric field, both suspensions exhibit a significant increase in shear stress and behave like a plastic material with a yield stress, the so-called ER effect. Compared to the pure LDH suspension, however, the GNS/LDH suspension exhibits higher shear stress at the equal electric field, indicating a stronger ER effect.

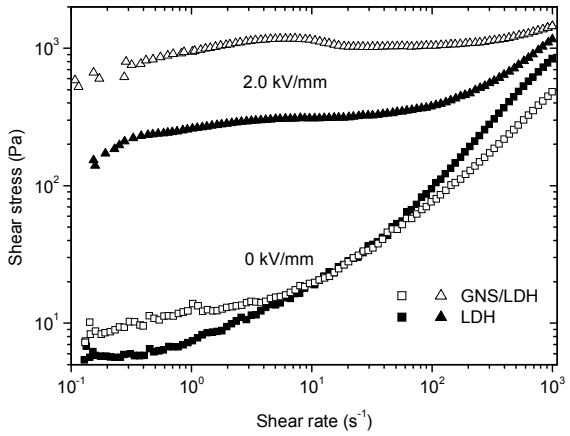

Fig. 9 Flow curves of shear stress vs. shear rate for 10wt% GNS/LDH suspension and pure LDH suspension under zero and 2 kV/mm of AC electric field with frequency of 1 kHz (ϕ =15 vol%, T=23°C).

Fig. 10 plots the typical ER efficiency of suspensions at 2 kV/mm of AC electric field with frequency of 1 kHz. The ER efficiency is important parameter for evaluating the change in ER behavior of fluids in the absence and presence of an electric field. It can be defined as $I=(\tau_E-\tau_0)/\tau_0$, where τ_E is the shear stress with an electric field and τ_0 is the shear stress before an electric field applied, respectively. As seen, the ER efficiency presents a decrease with increasing shear rate. This can be attributed to the fact that the gap-spanning fibrous-like ER structure is progressively destroyed with increasing shear rate and, as a result, their resistance to the flow decreases. However, it is noted that the ER efficiency of the GNS/LDH suspension is higher than that of the pure LDH suspension, indicating that the GNS/LDH composite does have stronger ER effect. According to the proposed ER mechanism,[45] the ER effect is strongly related to interparticle electrostatic interaction. Therefore, the stronger ER effect of the GNS/LDH composite should be attributed to the enhanced polarizability that has induced larger electrostatic interaction.

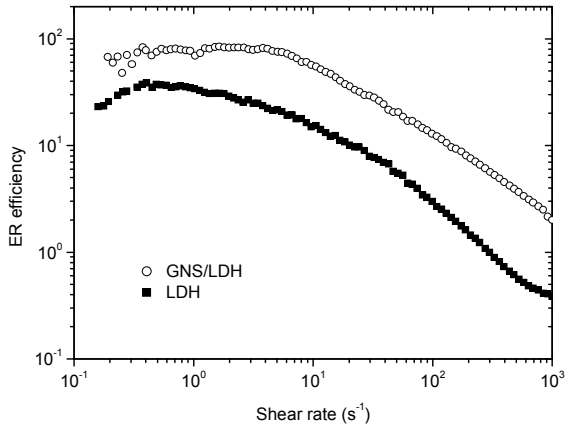

Fig. 10 Typical ER efficiency as a function of shear rate for 10wt% GNS/LDH suspension and pure LDH suspension at 2 kV/mm of AC electric field with frequency of 1 kHz (ϕ =15 vol%, T=23°C).

Fig. 11 shows the static yield stress (τ_s) as a function of electric field strength (E) for the 10 wt% GNS/LDH suspension and pure LDH suspension under AC electric field with frequency of 1 kHz. It can be found that, compared to the pure LDH suspension, the yield stress of the GNS/LDH suspension is higher, which is in accordance with the stronger ER effect of GNS/LDH suspension. The relationship of τ_s and E can be fitted by the power law relation of $\tau_s \propto E^{\alpha}$ with exponent α=1.86±0.05 for the pure LDH suspension and α=1.85±0.03 for the GNS/LDH suspension. It has been reported that the exponent α of ER suspensions is sensitive to the conductivity of oil, particle volume fraction, particle morphology, etc.[15] Therefore, the similar exponent value for both suspensions can be attributed to the fact that both suspensions have the same medium oil, particle volume fraction and particle morphology. In addition, the real leaking current density of GNS/LDH suspension is ~320 μA/cm^2 under 2 kV/mm of AC electric field, which is higher than ~280 μA/cm^2 of pure LDH suspension. This can be attributed to the enhanced conductivity due to the incorporation of conducting GNS.

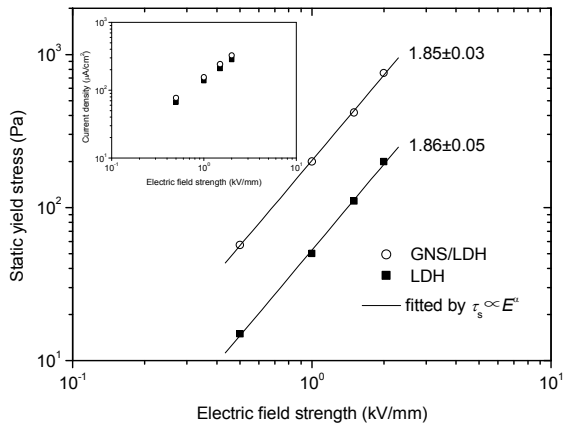

Fig. 11 Static yield stress and leaking current density (inset) as a function of electric field strength for 10wt% GNS/LDH suspension and pure LDH suspension under AC electric field with frequency of 1 kHz (ϕ=15 vol%, T=23°C).

Fig. 12 shows the static yield stress as a function of electric field frequency (f) for the 10 wt% GNS/LDH suspension and pure LDH suspension at 1.5 kV/mm of electric field. As the electric field frequency increases, the yield stress of the suspension of GNS/LDH composite increases, while the ER effect of pure LDH degrades. It indicates that, compared to pure LDH, the ER effect of GNS/LDH composite is not only stronger but also more active on exposure to AC electric fields. This characteristic may be related to the fact that the incorporation of the highly conducting GNS has not only enhanced the polarizability of LDH but also induced faster polarization rate (see Table 1). It has proposed that not only the polarizability but also the polarization rate of particles is important to the ER effect.[45] The former is related to the magnitude of interpaticle electrostatic interaction, while the latter is related to the reorganization of the destroyed ER structure under simultaneous effects of both electric and shearing fields. Under a DC electric field, both pure LDH and GNS/LDH composite can well reorganize their destroyed ER structures by shearing fields because their polarization rates are sufficient to response to DC electric field. Under an AC electric field, however, the reorganization of the destroyed ER structure requires ER particles to possess a faster polarization rate in order to match the frequency of external field. Since the polarization rate of pure LDH is slow, the particle polarization of pure LDH gradually becomes insufficient with the increase of electric field frequency and, as a result, the interparticle interaction and the ER effect decrease. On the contrary, the polarization rate of GNS/LDH composite is so fast that the particle polarization response can well match the frequency of external field and, as a result, the destroyed ER structure can be well reorganized and the ER response of GNS/LDH composite becomes better with the increase of electric field frequency.

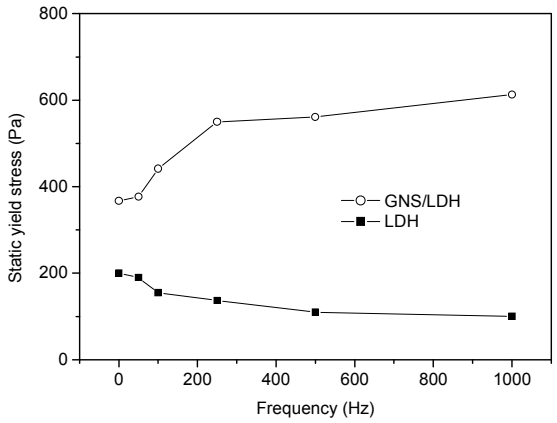

Fig. 12 Static yield stress as a function of electric field frequency for 10wt% GNS/LDH suspension and pure LDH suspension under 1.5 kV/mm of electric field (ϕ=15 vol%, T=23°C).

Table 2. Rheological properties of LDH and GNS/LDH suspensions (ϕ=15 vol%, T=23°C).

Material	τ_0(Pa) [a]	τ_E(Pa) [b]	I [c]
LDH	90	370	3.1
3wt% GNS/LDH	87	730	7.4
5wt% GNS/LDH	85	960	10.3
10wt% GNS/LDH	73	980	12.4
15wt% GNS/LDH	70	950	12.6

[a] τ_0 is the shear stress of suspensions at 100 s^{-1} in the absence of an electric field; [b] τ_E is the shear stress of suspensions at 100 s^{-1} in the presence of 2 kV/mm of AC electric field with 1 kHz; [c] $I=(\tau_E-\tau_0)/\tau_0$ is ER efficiency.

Finally, it is noted that the ER effect of the GNS/LDH composite is related to the GNS content. As shown in Table 2, the ER efficiency increases with increasing GNS content and seems to become saturate when the GNS content exceeds 10 wt%. However, the current density also continuously increases with increasing GNS content, indicating increased power consumption. When the GNS content is too high (>~20 wt%), the leaking current density of suspension exceeds the limitation of high-voltage generator. This may be attributed to the appearance of free GNS, which results in dielectric breakdown

or current percolation. Therefore, an appropriate content of GNS is the key to the versatile ER performance including high ER efficiency but relatively low current density.

Conclusions

By a simple one-pot hydrothermal method, we have prepared GNS/LDH composite dielectric nanoplates for use as novel 2D electro-responsive ER material. It has demonstrated that the LDH can provide electrically insulting effect for GNS, while conducting GNS can enhance the dielectric property of LDH. This allows the GNS/LDH composite to possess low conductivity but enhanced dielectric polarization. Under electric fields, the GNS/LDH composite shows stronger electro-responsive ER characteristic than that of pure LDH due to enhanced polarizability. Especially, the ER effect of GNS/LDH composite is more active on exposure to an AC electric field, which can be attributed to the fact that the incorporation of the highly conducting GNS not only enhances the polarizability of LDH but also induces faster polarization rate. Our result provides an approach to develop highly active 2D ER material by combining the advantages of conducting GNS and insulating layered inorganic.

Acknowledgements

This work is supported by the Program for New Century Excellent Talents in University of China, National Natural Science Foundation of China (no. 51272214), and NPU Foundation for Fundamental Research (no. JC20120247).

Notes and references

[a] *Smart Materials Laboratory, Department of Applied Physics, Northwestern Polytechnical University, Xi'an 710129, P. R. China. Fax: 86 29 88491000; Tel: 86 29 88431662; E-mail: jbyin@nwpu.edu.cn; xpzhao@nwpu.edu.cn*

1. K. S. Novoselov, A. K. Gaim, S. V. Morozov, D. Jiang, Y. Zhang, S. V. Dubonos, I. V. Grigorieva and A. A. Firsov, *Science*, 2004, **306**, 666.
2. V. Singh, D. Joung, L. Zhai, S. Das, S. I. Khondaker and S. Seal, *Prog. Mater Sci*, 2011, **56**, 1178.
3. N. Behabtu, J. R. Lomeda, M. J. Green, A. L. Higginbotham, A. Sinitskii, D. V. Kosynkin, D. Tsentalovich, A. N. G. Parra-Vasquez, J. Schmidt, E. Kesselman, Y. Cohen, Y. Talmon, J. M. Tour and M. Pasquali, *Nature Nanotechnology*, 2010, **5**, 406.
4. S. S. Jyothirmayee Aravind and S. Ramaprabhu, *J. Appl. Phys*, 2011, **110**, 124326.
5. W. L. Zhang, B. J. Park and H. J. Choi, *Chem. Commun.*, 2010, **46**, 5596.
6. H. T. Hu,X. B. Wang, J. C. Wang, F. M. Liu, M. Zhang and C. H. Xu, *Appl. Surf. Sci*, 2011, **257**, 2637.
7. W. L. Zhang, Y. D. Liu and H. J. Choi, *J. Mater. Chem*, 2011, **21**, 6916.
8. J. B. Yin, X. X. Wang, R. T. Chang and X. P. Zhao, *Soft Matter*, 2012, **8**, 294.
9. J. B. Yin, R. T. Chang, Y. Kai and X. P. Zhao, *Soft Matter*, 2013, **9**, 3910.
10. J. B. Yin, R. T. Chang, Y. J. Shui and X. P. Zhao, *Soft Matter*, 2013, **9**, 7468.
11. J. Y. Hong, E. Lee and J. Jang, *J. Mater. Chem. A*, 2013, **1**, 117.
12. W. J. Wen, X. X. Huang, S. H. Yang, K. Q. Lu and P. Sheng, *Nat. Mater*, 2003, **2**, 727.
13. J. B. Yin and X. P. Zhao, *Nanotechnology*, 2006, **17**, 192.
14. C. Lin and J. W. Shan, *Phys. Fluids*, 2007, **19**, 121702.
15. J. B. Yin, X. P. Zhao, X. Xia, L. Q. Xiang and Y. P. Qiao, *Polymer*, 2008, **49**, 4413.
16. M. M. Ramos-Tejada, M. J. Espin, R. Perea and A. V. Delgado, *J. Non-Newtonian Fluid Mech*, 2009, **159**, 34.
17. J. B. Yin, X. Xia, L. Q. Xiang and X. P. Zhao, *J. Mater. Chem.*, 2010, **20**, 7096.
18. Y. D. Liu, F. F. Fang and H. J. Choi, *Mater. Lett.*, 2010, **64**, 154。
19. Y. C. Cheng, K. Wu, F. H. Liu, J. J. Guo, X. H. Liu, G. J. Xu and P. Cui, *ACS Appl. Mater. Interfaces*, 2010, **2**, 621.
20. J. H. Wu, T. Jin, F. H. Liu, J. J. Guo, P. Cui, Y. C. Cheng and G. J. Xu, *J. Mater. Chem. C*, 2014, **2**, 5629.
21. M. Sedlacik, M. Mrlik, Z. Kozakova, V. Pavlinek and I. Kuritka, *Colloid Polym. Sci.,* 2013, **291**, 1105
22. S. Almajdalawi, V. Pavlinek, M. Mrlik, Q. Cheng and M. Sedlacik, *J. Phys. Conf. Series,* 2013, **412**, 012003
23. A. Schönhals, H. Goering, F. R. Costa, U. Wagenknecht and G. Heinrich, *Macromolecules*, 2009, **42**, 4165.
24. F. Leroux, A. Illaik, T. Stimpfling, A. Troutier-Thuilliez, S. Fleutot, H. Martinez, J. Cellier and V. Verney, *J. Mater. Chem.,* 2010, **20**, 9484.
25. P. J. Purohit, J. E. Huacuja-Sánchez, D. Y. Wang, F. Emmerling, A. Thúnemann, G. Heinrich and A. Schönhals, *Macromolecules*, 2011, **44**, 4342
26. F. Leroux, K. Chabrol, S. Thérias, J. Gardette and A. de Roy, *Eur. J. Inorg. Chem.,* 2012, **32**, 5332.
27. E. V. Korobko, *J. Intell Mater. Syst. Struct.*, 1992, **3**, 268.
28. H. J. Choi, J. W. Kim, J. Joo and M. S Jhon, *Synth. Met.*, 2001, **121**, 1325.
29. J. Lu and X. P. Zhao, *J. Mater. Chem.*, 2002, **12**, 2603
30. D. C. Marcano, D. V. Kosynkin, J. M. Berlin, A. Sinitskii, Z. Z. Sun, A. Slesarev, L. B. Alemany, W. Lu and J. M. Tour, *ACS Nano*, 2010, **4**, 4806.
31. T. Wen, X. Wu, X. Tan, X. Wang and A. Xu, *ACS Appl. Mater. Interfaces* 2013, **5**, 3304.
32. J. B. Yin, X. Xia, L. Q. Xiang and X. P. Zhao, *Smart Mater. Struct.*, 2011, **20,** 015002.
33. M. Whittle, W. A. Bullough, D. J. Peel and R. Froozian, *Phys. Rev. E*, 1994, **49,** 5249.
34. W. L. Zhang, Y. D. Liu and H. J. Choi, *J. Mater. Chem.*, 2011, **21**, 6916.
35. J. de Vicente, F. Vereda and J. P. Segovia-Gutierrez, *J. Rheol.*, 2010, **54**, 1337.
36. Z. Zhang, F. Xiao,Y. Guo, S. Wang and Y. Liu, *ACS Appl. Mater. Interfaces,* 2013, **5**, 2227
37. J. L. Gunjakar, I. Y. Kim, J. M. Lee, N.-S. Lee and S.-J. Hwang, *Energy Environ. Sci.*, 2013, **6**, 1008.
38. A. Garcia-Gallastegui, D. Iruretagoyena, V. Gouvea, M. Mokhtar, A. M. Asiri, S. N. Basahel, S. A. Al-Thabaiti, A. O. Alyoubi, D. M. Chadwick and S. P. Shaffer, *Chem. Mater.*, 2012, **24**, 4531.
39. C. Navarro, R. T. Weitz, A. M. Bittner, M. Scolari, A. Mews, M. Burghard and K. Kern, *Nano Lett.,* 2007, **7**, 3499.
40. H. Li, G. Zhu, Z. Liu, Z. Yang and Z. Wang, *Carbon*, 2010, **48**, 4391.

41. J. L. Gunjakar, I. Y. Kim, J. M. Lee, N. Lee and S. Hwang, *Energy Environ. Sci.,* 2013, **6**, 1008.
42. L. Davis, *J. Appl. Phys.*, 1992, **72**, 1334.
43. C. Huang and Q. M. Zhang, *Appl. Phys. Lett.*, 2003, **82**, 3502.
44. G. Schmidt, A. I. Nakatani and C.C. Han, *Rheol. Acta,* 2002, **41**, 45.
45. F. Ikazaki, A. Kawai, K. Uchida, T. Kawakami, K. Edmura, K. Sakurai, H. Anzai and Y. Asako, *J. Phys. D: Appl. Phys.,* 1998, **31,** 336.

Graphic abstract

Dielectric nanoplates composed of graphene nanosheet/layered double-hydroxide (GNS/LDH) composite were prepared, which showed enhanced electro-responsive characteristic compared to pure LDH due to improved dielectric polarization.